The theory of far-infrared optics of layered antiferromagnets

1995 J. Phys.: Condens. Matter 7 2717

(http://iopscience.iop.org/0953-8984/7/14/011)

J. Phys.: Condens. Matter 7 (1995) 2717–2730. Printed in the UK

The theory of far-infrared optics of layered antiferromagnets

Kamsul Abraha†‡ and D R Tilley§

† Department of Physics, University of Essex, Colchester CO4 3SQ, UK
‡ Jurusan Fisika FMIPA, Universitas Gadjah Mada, Yogyakarta 55281, Indonesia
§ School of Physics, Universiti Sains Malaysia, 11800 USM Penang, Malaysia

Received 13 December 1994

Abstract. We present a full theoretical discussion of the surface polaritons, ATR and oblique incidence reflectivity spectra of layered antiferromagnets. The results apply equally to a large class of easy-plane magnetic systems including artificial magnetic superlattices with antiferromagnetic coupling. It has recently been argued that the conventional calculation of the RF permeability tensor μ is incorrect and should be replaced by a calculation that is consistent with macroscopic electrodynamics. Our computed spectra for NiO lead to the conclusion that the form of μ can be established by comparison with experimental far-infrared spectra.

1. Introduction

We have recently [1] reconsidered the calculation of the RF permeability tensor μ for easy-plane layered antiferromagnetic such as NiO (Néel temperature $T_N = 523$ K) with simple NaCl structure. With a magnetic field applied parallel to the easy planes, the orientation of the sublattice moments is as shown in figure 1. The conventional calculation of μ in a magnetic crystal [2] involves finding the linear response of the spin system to an applied RF field $\boldsymbol{h}\exp(-i\omega t)$. However, we argue that this is not correct for an easy-plane antiferromagnet. The argument applies equally to some superlattices in which successive planes order as in figure 1. We propose [1], by analogy with the effective-medium theory of magnetic superlattices [3, 4], that the correct procedure is to find the response to the components of $\boldsymbol{h}$ parallel to the planes but to the component of $\boldsymbol{b}$ normal to the planes. The physical argument is that in macroscopic electrodynamics these are the components that are continuous from layer to layer. The result of this 'h/b' analysis is that μ takes the form

$$\mu = \begin{pmatrix} \mu_{xx} & \mu_{xy} & 0 \\ -\mu_{xy} & \mu_{yy} & 0 \\ 0 & 0 & \mu_{zz} \end{pmatrix} \tag{1}$$

with

$$\mu_{xx} = 1 + 4\pi\gamma^2 M_s\left(H_a + 2H_e\right)/\left(\omega_+^2 - \omega^2\right) \tag{2}$$

$$\mu_{yy} = 1 + 4\pi\gamma^2 M_s H_0 \cos\alpha/\left(\omega_+^2 - \omega^2\right) \tag{3}$$

$$\mu_{xy} = -i4\pi\gamma M_s\omega/\left(\omega_+^2 - \omega^2\right) \tag{4}$$

$$\mu_{zz} = 1 + 4\pi\gamma^2 M_s\left(M_a + 4\pi M_s\right)\sin^2\alpha/\left(\omega_d^2 - \omega^2\right). \tag{5}$$

0953-8984/95/142717+14$19.50

The resonance frequencies in these expressions are given by

$$\omega_+ = \gamma\left[H_0\left(H_0 + H_a \cos\alpha\right)\right]^{1/2} \tag{6}$$

and

$$\omega_d = \gamma\left[2H_e\left(H_a + 4\pi M_s\right)\sin^2\alpha\right]^{1/2}. \tag{7}$$

Here α is the canting angle as shown in figure 1. For bulk crystals, $\cos\alpha = H_0/2H_e$. The result of the conventional 'applied h' analysis [1] is that μ_{xx}, μ_{xy} and μ_{yy} take the same form, but in the expression for μ_{zz}, $H_a + 4\pi M_s$ is replaced by H_a and ω_d by ω_-, where

$$\omega_- = \gamma\left(2H_eH_a\sin^2\alpha\right)^{1/2}. \tag{8}$$

In other words, by comparison with the expression for ω_-, ω_d contains the demagnetizing factor $4\pi M_s$. The question that arises is how the difference between the two expressions for μ_{zz} can be tested experimentally. We discuss this by reference to calculated dispersion and oblique incidence reflectivity curves. We may mention that the current literature values for NiO, derived from antiferromagnetic resonance (AFMR) transmission measurements [5–7], are $H_e = 31.83$ T and $H_a = 15.6$ T, corresponding to an AFMR frequency at 36.6 cm^{-1}. This mode has also been investigated by other techniques, including inelastic neutron scattering [8] and recently by Raman scattering [9]. For available applied field H_0 in a laboratory, ω_+ is of the order of up to 10 cm^{-1} whereas ω_- and ω_d are in the far-infrared region accessible to Fourier transform spectroscopy. The lower mode (ω_+) was claimed to appear in a Brillouin scattering study of NiO [10].

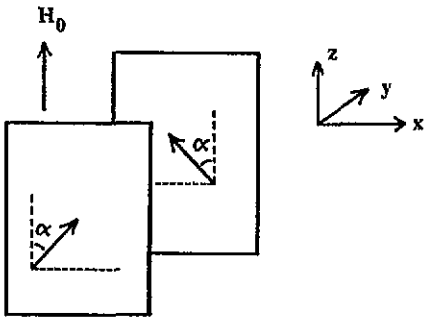

Figure 1. The spin configuration in the layered antiferromagnet NiO. The moments within one (zx) plane, i.e. a (111) plane, are aligned and in the absence of an applied field moments on neighbouring planes are antiparallel. In the presence of a field the moments turn towards H_0 through an angle α [1]. H_0 is in the (111) plane.

Theoretical consideration of the question is timely because of the recent development of a high-resolution Fourier transform spectrometer for studies of magnetic materials [11]. So far this instrument has been applied [12, 13] to a detailed study of the oblique incidence reflectivity of the uniaxial antiferromagnet FeF_2 (Néel temperature $T_N = 78$ K). In the experimental arrangement the magnetic field is vertical and the plane of incidence horizontal; the usual angle of incidence is 45°. The next stage of instrumental development is the introduction of a prism so as to enable attenuated total reflection (ATR) measurements to

be carried out in the Otto configuration, in which an air gap separates the prism from the sample. In this technique, the ATR scan line in the ω–q plane is $q = \varepsilon_p^{1/2}\,(\omega/c)\sin\phi$, where ε_p is the prism dielectric constant and ϕ is the angle of incidence in the prism. Dips are seen when the scan line crosses a surface polariton dispersion curve [2, 11], so this technique gives direct access to the surface polaritons. Our theoretical estimate [15] is that an Si prism ($\varepsilon_p = 11.56$) with $\phi = 45°$ should be suitable.

The plan of this paper is as follows. In section 2 we derive and illustrate the surface polariton dispersion curves. Sections 3 and 4 are concerned specifically with the question of the alternative forms of μ_{zz}; we show calculated ATR and reflectivity curves. A general discussion and conclusions are presented in section 5.

2. Surface polaritons

We consider the interface at $y = 0$ between vacuum ($y < 0$) and the sample ($y > 0$), and we follow the usual derivation [2] of the surface polariton dispersion curve. This means first finding solutions of Maxwell's equations that decay away from the interface and second applying the electromagnetic boundary conditions to find the dispersion relation. In the medium the RF field $\boldsymbol{H}$ satisfies

$$\nabla^2\boldsymbol{H} - \nabla(\nabla\cdot\boldsymbol{H}) + \varepsilon\left(\omega^2/c^2\right)\boldsymbol{\mu}\cdot\boldsymbol{H} = \boldsymbol{0}. \tag{9}$$

We require a solution that propagates as a plane wave in the x direction decays as in the y direction:

$$\boldsymbol{H} = \left(H_{1x},\ H_{1y},\ H_{1z}\right)\exp\left(-\alpha_1 y\right)\exp(iqx - i\omega t) \qquad (y > 0). \tag{10}$$

Substitution of equation (10) into equation (9) gives three homogeneous, linear equations for the components of $\boldsymbol{H}$, namely

$$\begin{bmatrix} \alpha_1 + k^2\mu_{xx} & iq\alpha_1 + k^2\mu_{xy} & 0 \\ iq\alpha_1 - k^2\mu_{xy} & -q^2 + k^2\mu_{yy} & 0 \\ 0 & 0 & \alpha_1 - q^2 + k^2\mu_{zz} \end{bmatrix}\begin{bmatrix} H_{1x} \\ H_{1y} \\ H_{1z} \end{bmatrix} = 0 \tag{11}$$

with $k^2 = \varepsilon\omega^2/c^2$. Here, ε is the dielectric constant of the magnetic crystal. It is seen from equation (11) that the solutions separate into the two polarizations (H_{1x}, H_{1y}, 0) and (0, 0, H_{1z}), which we denote as s and p, as previously [12, 13]. This nomenclature agrees with the convention that in s polarization the RF $\boldsymbol{E}$ field is transverse to the plane of incidence. The spatial decay constant α_1 is then given by

$$\alpha_1^2\mu_{yy} - q^2\mu_{xx} + k^2\left(\mu_{xx}\mu_{yy} + \mu_{xy}^2\right) = 0 \qquad \text{s polarization} \tag{12}$$

$$\alpha_1^2 - q^2 + k^2\mu_{zz} = 0 \qquad \text{p polarization.} \tag{13}$$

In the vacuum, the corresponding wave equation for the RF $\boldsymbol{H}$ field is

$$\nabla^2\boldsymbol{H} + \omega^2/c^2\boldsymbol{H} = \boldsymbol{0} \tag{14}$$

with a plane wave solution

$$\boldsymbol{H} = \left(H_{0x},\ H_{0y},\ H_{0z}\right)\exp\left(\alpha_0 y\right)\exp(iqx - i\omega t) \qquad (y < 0) \tag{15}$$

so that in either polarization the decay constant α_0 is given by

$$\alpha_0^2 = q^2 - \omega^2/c^2. \tag{16}$$

We now apply the conditions of continuity of the parallel components H_z and E_x. For p polarization the latter is given by

$$E_{0x} = \pm i\alpha_n H_{0z}/(\varepsilon_0 \varepsilon_n \omega) \qquad n = 0,\ 1 \tag{17}$$

where the + sign applies in vacuum ($n = 0$, $\varepsilon_0 = 1$, $y < 0$) and the − sign in the medium ($n = 1$, $\varepsilon_1 = \varepsilon$, $y > 0$); H_{0z} is the common value of H_z at the interface. Putting $E_{0x} = E_{1x}$ we find

$$\alpha_1 = -\varepsilon\alpha_0. \tag{18}$$

Now a condition for equations (10) and (15) to describe a surface mode is that both α_0 and α_1 are real and positive. Usually, the magnetic resonances do not coincide with dielectric resonances, so consequently ε is also positive. Thus equation (18) has no solution and there is no surface polariton in p polarization. This result is surprising, or at least we find it so, since a strong magnetic resonance is seen in p polarization oblique incidence reflection off FeF_2 in this geometry [12]. Since μ_{zz} appears only in the expression (13) for α_1, in p polarization, this means that experiments aimed specifically at surface polaritons cannot resolve the question of the proper form of μ_{zz} in NiO-type structures. The corresponding ATR calculation described in section 3 verifies the nonexistence of this surface mode.

Figure 2 shows an example of the dispersion curves for bulk p-polarized polaritons in NiO. The dispersion relation is given by $q^2 = \varepsilon\mu_{zz}\omega^2/c^2$. This is even in q so that bulk mode propagation is reciprocal. Here we show the results with μ_{zz} derived from a conventional analysis in figure 2(*a*) and from an h/b analysis in figure 2(*b*). The bulk polariton dispersion curves are the curved lines in each figure. In discussion of oblique incidence reflectivity or ATR it is convenient to interpret figures of this kind as ω versus q where q is the in-plane wavevector component. In this case bulk polariton modes can occur throughout the *bulk continuum* region shown shaded in figure 2(*a*) and (*b*). The main distinction between the two figures is a difference of about 1 cm^{-1} in the location of the frequency gap between the two bulk continuum regions. For future reference, the ATR scan line (a), the oblique incidence (45°) reflectivity scan line (b) and the vacuum light line(c) are also drawn. In either case, the reflectivity scan line passes through a very narrow gap around 33 or 34 cm^{-1} between the bulk continuum regions. Within a bulk continuum the incident light can generate bulk polaritons so the reflectivity R is less than unity. In the gap, however, no coupling to bulk polaritons occurs so the gap is a *reststrahl*-like region with $R \approx 1$. Therefore, in the absence of a surface mode, we may expect that the oblique incidence reflectivity in p polarization will give very sharp peaks in this band. This is the case as will be made clear in section 4.

We now turn to s polarization and it is convenient to work in terms of the electric field amplitude E_z, which is continuous at the interface. The other continuous field component H_x is found to be

$$H_{1x} = \left[\left(i\alpha_1\mu_{yy} + q\mu_{xy}\right)/\left(\mu_{xx}\mu_{yy} + \mu_{xy}^2\right)\right]E_z/\mu_0\omega \qquad y > 0 \tag{19}$$

and

$$H_{0x} = -i\alpha_0 E_z/(\mu_0\omega) \qquad y < 0. \tag{20}$$

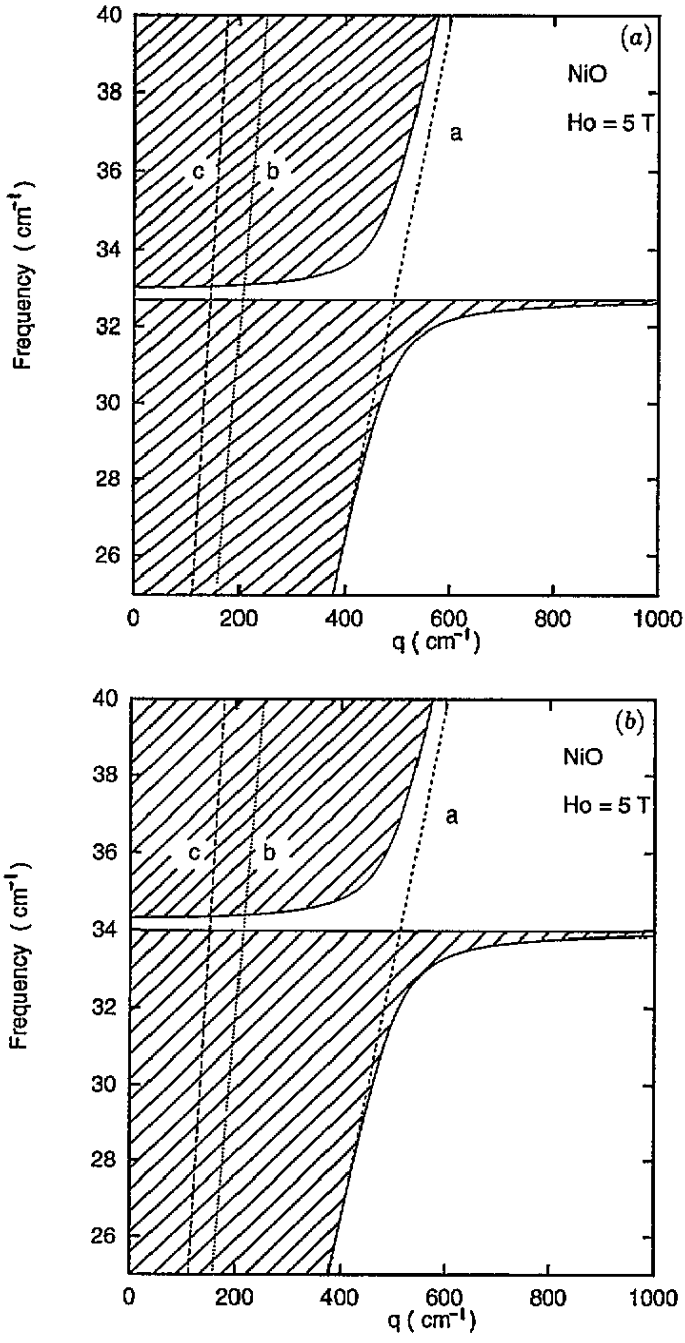

Figure 2. The dispersion curves for bulk (shaded regions) p-polarized polaritons on NiO. We have made use of the magnetic permeability tensor element μ_{zz} derived by different methods: (*a*) the constant-h or conventional method; (*b*) the h/b method. In both sets of curves, three scan lines are also shown: the ATR scan line with $\phi = 45°$ and $\varepsilon_p = 11.56$ (line a), the 45°-reflectivity scan line (line b) and the vacuum light line (line c). Other magnetic parameters are taken from [5] and [7].

Equating these two components, we find the dispersion relation to be

$$\alpha_0\mu_V + (\mu_{yy}\alpha_1 - iq\mu_{xy})/\mu_{xx} = 0 \tag{21}$$

where μ_V is the Voigt permeability for this geometry,

$$\mu_V = \mu_{yy} + \mu_{xy}^2/\mu_{xx} \tag{22}$$

and

$$\alpha_1^2 = \mu_{xx}(q^2 - \varepsilon\mu_V\omega^2/c^2)/\mu_{yy}. \tag{23}$$

Non-reciprocal propagation of the surface polaritons [16] is evident in the appearance of the linear term $q\mu_{xy}/\mu_{xx}$ in equation (21), which means that $\omega(-q) \neq \omega(q)$. The required dispersion relations for surface polaritons are given by the values of ω and q that satisfy equation (21) and also give real and positive values for α_0 in (16) and α_1 in (23). With $\alpha_1 = 0$, in addition, we obtain from (23) the dispersion relation for the bulk modes, namely $q^2 = \varepsilon\mu_V\omega^2/c^2$. This is even in q, so bulk mode propagation is reciprocal.

For later purposes, it will be useful to consider briefly the properties of the Voigt permeability μ_V near the vicinity of the magnetic resonance frequency ω_+. Using equations (2)–(5) in equation (22) we find that

$$\mu_V(\omega) = (\omega^4 + A\omega^2 + B)/(\omega^2 - \omega_1^2)(\omega^2 - \omega_2^2). \tag{24}$$

Here, the exact forms of the constants A and B are determined by the magnetic parameters of the antiferromagnet. Therefore, in contrast to the ferromagnet in the same geometry [17], the Voigt permeability given by (24) has two poles and two zeros. The presence of these poles, in particular, leads to the existence of three bulk continua where bulk polaritons may exist and in the frequency gaps ($\mu_V < 0$) between these bands we may find surface polaritons. It is a matter of algebra to find that the pole and zero frequencies are

$$\omega_1 = \omega_+ \qquad \omega_2 = \omega_+\left[1 + 4\pi\gamma^2 M_s(H_a + 2H_e)/\omega_+^2\right]^{1/2} \qquad \text{(poles)} \tag{25a}$$

$$\omega_0^{\pm} = \left[\omega_+^2 + 2\pi\gamma M_s(C \pm D)\right]^{1/2} \qquad \text{(zeros)} \tag{25b}$$

where

$$C = \gamma(H_a + 2H_e + H_0\cos\alpha) \tag{25c}$$

$$D = \left[4\omega_+^2 + \gamma^2(H_a + 2H_e - H_0\cos\alpha)^2 + 4\pi\gamma M_s\{2\gamma(H_a + 2H_e + H_0\cos\alpha) + 4\pi\gamma M_s\}\right]^{1/2}. \tag{25d}$$

We should mention at this point that the existence of these poles and zeros was not clearly indicated in the works reported previously [12, 18].

In figure 3 we plot the dispersion curves in s polarization for bulk and surface polaritons on NiO with the spin configuration depicted in figure 1. We find in this case that the surface modes are all virtual with no magnetostatic limits and they are markedly non-reciprocal. Each of these modes starts at a certain point on the vacuum light line and terminates at a finite value of q in the bulk continuum. In order to compare to future experimental work that may soon be available [11–13], some ATR scan lines with a fixed angle of incidence of 45° (as will be the favourable case in an experimental run) are also drawn. As indicated in the figure, ATR dips may be expected when the scan lines cross the surface polariton dispersion curves. The frequency band where the middle bulk continuum exists ($\omega_1 < \omega < \omega_2$) is remarkably wide. We may expect that oblique incidence reflectivity [12] in s polarization will give broad dips in this band. This indeed is the case as will be made clear in section 4.

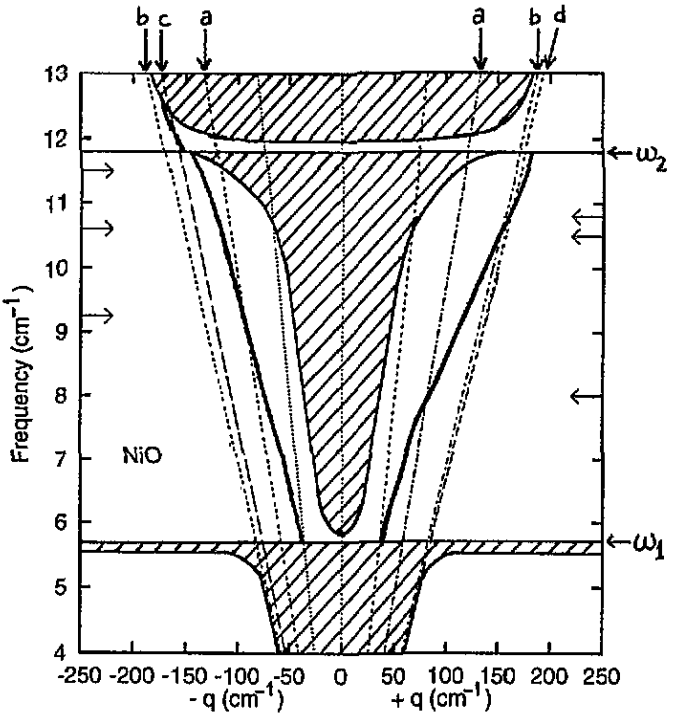

Figure 3. The dispersion curves for bulk (shaded regions) and surface s-polarized (solid lines) polaritons on the layered antiferromagnet NiO. The applied field is 5 T. Some ATR scan lines with $\phi = 45°$ are also shown for $\varepsilon_p = 5.29$ (SiO_2) (a), $\varepsilon_p = 10.55$ (sapphire) (b), $\varepsilon_p = 9.0$ (c) and $\varepsilon_p = 11.22$ (d). The arrows on the vertical axis indicate frequencies of ATR dips discussed later in section 3. The surface modes have no magnetostatic analogue, i.e. they are virtual modes. ω_1 and ω_2 are given by equation (25).

3. Attenuated total reflection (ATR)

We consider an ATR arrangement in the Otto configuration, as illustrated in figure 4. Since there is no surface polariton in p polarization we first deal with a s polarization. We do not repeat the standard details of the ATR calculation, which are given elsewhere [2, 15], so we need only quote the result:

$$R = \left|\left[k_\perp(1+f) - i\alpha_0(1-f)\right]/\left[k_\perp(1+f) + i\alpha_0(1-f)\right]\right|^2 \tag{26}$$

where

$$k_\perp = \varepsilon_p^{1/2}(\omega/c)\cos\phi \qquad k_\parallel = \varepsilon_p^{1/2}(\omega/c)\sin\phi \tag{27}$$

$$f = \left[(i\alpha_0 - \alpha)/(i\alpha_0 + \alpha)\right]\exp(-2\alpha_0 d) \qquad \alpha = (i\alpha_1\mu_{xy} + k_\parallel\mu_{xy})/(\mu_y\mu_{xx}). \tag{28}$$

The inverse decay lengths α_0 and α_1 were defined previously in equations (16) and (23). As mentioned in section 1, ATR spectroscopy should prove effective in probing surface modes, as has been the case in semiconductor superlattices [14]. In typical far-infrared measurements, the angle of incidence ϕ is fixed and the frequency ω is scanned along the

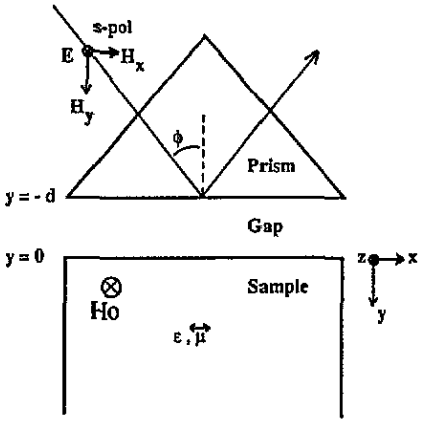

Figure 4. The geometry for the ATR calculation. Light is incident inside a prism of dielectric constant ε_p at an angle $\phi > \phi_c$, where ϕ_c is the critical angle for total internal reflection. The prism is separated from the sample by an air gap of thickness d.

scan line $k_{\parallel} = \varepsilon_p^{1/2}\,(\omega/c)\sin\phi$. In this work, we choose $\phi = 45°$ which is consistent with our reflectivity measurements [12, 13]. It is necessary to include a damping parameter Γ in the ATR calculation and we do this by the replacement $\omega \to \omega + i\Gamma$.

We present in figures 5–7 some ATR curves for surface polaritons of NiO with the dispersion relations already shown in figure 3. The geometry for the ATR calculation is given by figure 4.

Figure 5 shows the ATR curves for NiO with the scan line specified by $\varepsilon = 5.29$ and $\phi = 45°$, that is, line a on both $+q$ and $-q$ sides of the dispersion diagram in figure 3. The reflectivity is clearly non-reciprocal. With a moderate value of damping $\Gamma = 0.05\ \text{cm}^{-1}$ we find very sharp ATR dips with linewidth of the order of 0.2–0.3 cm^{-1}. As seen in figure 3, the scan line at the low-frequency region enters a bulk continuum and consequently gives $R < 1$ in this region.

Using values of ε_p corresponding to the ATR scan lines in figure 3 with a fixed value 45° for ϕ, we plot the ATR spectra in figure 6(a) for the $+q$ modes and figure 6(b) for $-q$ modes. Again with damping of 0.05 cm^{-1} we find sharp dips with linewidth of the same order as those shown in figure 5. The positions of these dips are at the scan line crossing frequencies indicated in figure 3. The frequencies at which the ATR dips are found are at the low-frequency end of the range of a standard far-infrared Fourier transform spectrometer. We believe that after some instrumental improvements [19] the ATR modes shown here should be detectable, as proved to be the case in semiconductor superlattices [14].

Finally, we consider an ATR calculation in the Otto configuration, as illustrated in figure 4 except that the incident beam is now in p polarization. An expression for the reflectivity can be derived as before. The result is given by

$$R = \left|\left[k_\perp(1+h) - i\varepsilon_p\alpha_0(1-h)\right]/\left[k_\perp(1+h) + i\varepsilon_p\alpha_0(1-h)\right]\right|^2 \tag{29}$$

where

$$h = \left[(\varepsilon\alpha_0 - \alpha_1)/(\varepsilon\alpha_0 + \alpha_1)\right]\exp(-2\alpha_0 d). \tag{30}$$

The quantities α_0 and α_1 are given by equations (16) and (23) respectively.

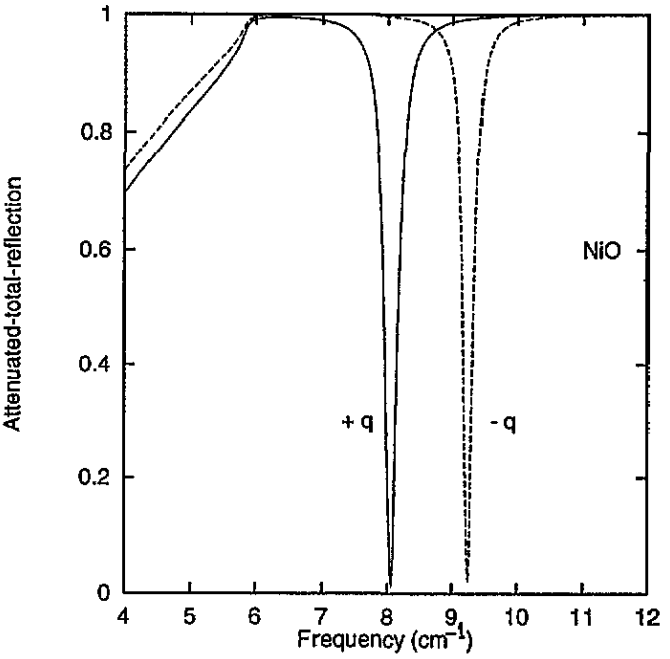

Figure 5. The computed ATR spectra in s polarization for surface polaritons of NiO whose dispersion curves are shown in figure 3. Parameters are given by $d = 340$ μm, $\phi = 45°$, $\Gamma = 0.05$ cm^{-1}, $\varepsilon_p = 5.29$ (associated with the scan line a indicated in figure 3) and $H_0 = 5$ T.

Figure 7 shows an example of the ATR curves for NiO, which can be understood by reference to the scan line a shown in figure 2. As mentioned before, there are no surface polaritons in p polarization. Consequently, the dips shown in figure 7 are merely due to coupling to bulk modes. At the low-frequency region the scan line falls in a region where bulk polaritons cannot exist so $R \approx 1$. For $\omega \approx 26$ cm^{-1} the scan line enters a bulk continuum and R drops slowly. Finally, for $\omega > \omega_-$ (curve A) or $\omega > \omega_d$ (curve B) the scan line is entirely in a broad *reststrahl* region with no surface modes and consequently R increases rapidly to $R \approx 1$.

4. Oblique incidence reflectivity

The second technique that might in principle test the position of the resonance in μ_{zz} is oblique incidence reflectivity. The experimental geometry is figure 4 without the prism. The resonances at ω_d for the h/b method (equation (7)) and ω_- for the conventional method (equation (8)) can be seen in p polarization oblique incidence reflectivity whereas the resonance at ω_+ for both methods is seen in s polarization. The reflectivity [12, 13] is $R = |(1-r)/(1+r)|^2$, where

$$r = \left[\left(\varepsilon\mu_s - \varepsilon_a \sin^2\phi\right)^{1/2}\varepsilon_a^{1/2}\varepsilon \sin\phi - \mu_{xy}\varepsilon^2\right]/\left[\mu_{xx}\varepsilon\varepsilon_a \sin\phi \cos\phi - \varepsilon\mu_{xy}\left(\varepsilon\mu_s - \varepsilon_a \sin^2\phi\right)^{1/2}\varepsilon_a^{1/2}\cos\phi\right] \qquad \text{(s polarization)} \tag{31}$$

and

$$r = \varepsilon_a^{1/2}\varepsilon \cos\phi/\left(\varepsilon\mu_{zz} - \varepsilon_a \sin^2\phi\right)^{1/2} \qquad \text{(p polarization)} \tag{32}$$

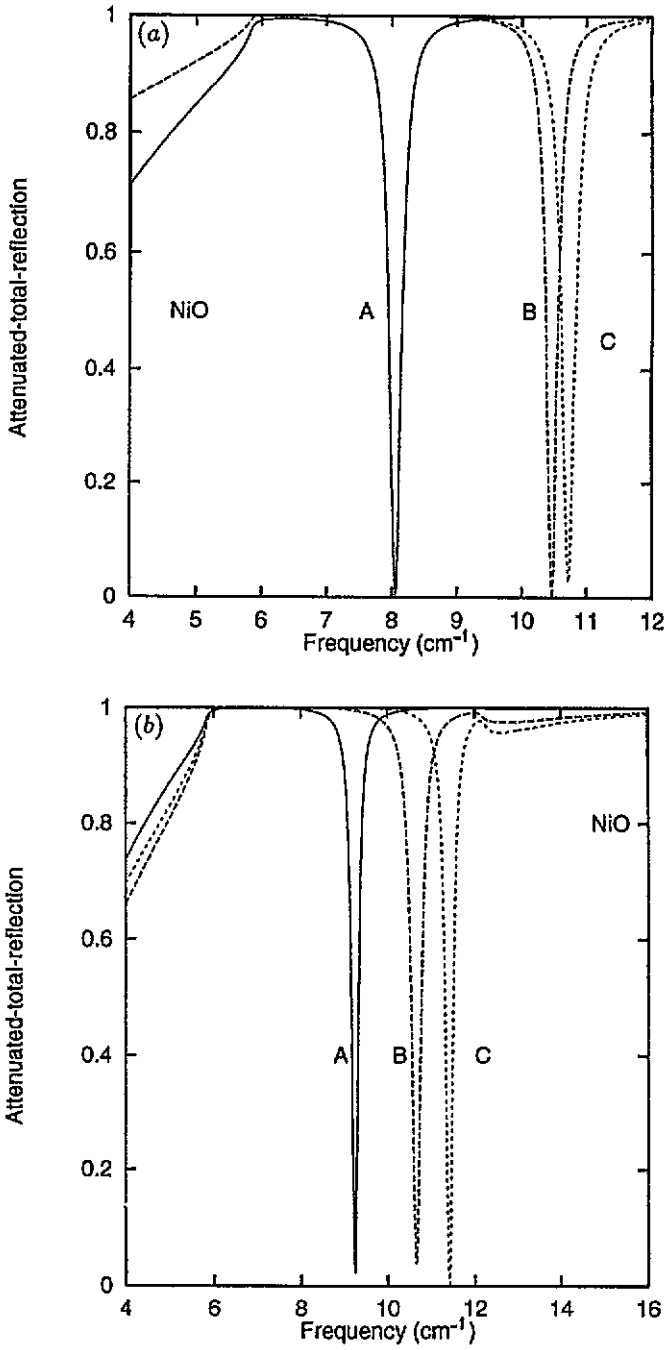

Figure 6. (*a*) The computed ATR spectra in s polarization of NiO using the scan lines a, b and d on the $+q$ side of the dispersion diagram depicted in figure 3. Labels on the graph stand for A, $\epsilon_p = 5.29$, $d = 350$ μm; B, $\epsilon_p = 10.55$, $d = 150$ μm and C, $\epsilon_p = 11.22$, $d = 118$ μm. (*b*) Analogous to (*a*) on the $-q$ side. A, $\epsilon_p = 5.29$, $d = 340$ μm; B, $\epsilon_p = 7$, $d = 200$ μm and C, $\epsilon_p = 8$, $d = 175$ μm. In both (*a*) and (*b*), $\Gamma = 0.05$ cm^{-1}.

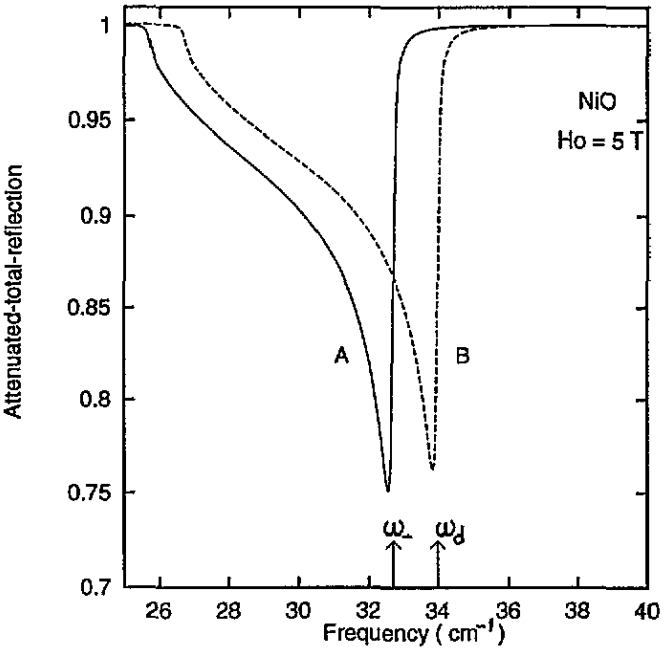

Figure 7. The computed ATR spectra of NiO in p polarization, given by equation (29). A, constant-h or conventional analysis; B, h/b analysis. Parameters are given by $d = 10$ μm, $\phi = 45°$, $\Gamma = 0.05$ cm^{-1} and $\varepsilon_p = 11.56$ (Si). The resonance frequencies ω_- and ω_d are indicated by the arrows.

where

$$\mu_s = \mu_{xx} + \mu_{xy}^2/\mu_{yy} + \left(1 - \mu_{xx}/\mu_{yy}\right)\varepsilon_a \sin^2 \phi/\varepsilon. \tag{33}$$

Here ε_a is the dielectric constant of the medium of incidence, ε the dielectric constant of the magnetic crystal and ϕ the angle of incidence. Thus, theoretically, the difference between the two expressions for μ_{zz} is seen from the p polarization spectra shown in figure 8 with separate features; actually the experiment can only give one of these spectra with a single resonance frequency, either ω_- or ω_d. Both sets of reflectivity curves can be understood by reference to the scan line b depicted in figure 2. The curves start at the low-frequency region with $R < 1$ since the scan line falls in a bulk continuum. As the frequency increases the scan line enters a narrow *reststrahl* region where coupling to bulk modes cannot occur. As a result, we find very sharp peaks with $R \to 1$ within this band. At the high-frequency region the scan line finally enters a bulk continuum and R decreases rapidly. As seen in figure 8, the resonance frequency shifts slightly to higher frequency with increasing field.

The resonance frequency, either ω_- or ω_d, may be obtained from a measured spectrum. As shown in equation (7) or (8), this frequency depends on the exchange and anisotropy fields H_e and H_a as well as on the sublattice magnetization M_s. Therefore if independent series of measurements of those fields and M_s are available, for example s polarization reflectivity in a range of fields, we propose that far-infrared spectroscopy developed so far for studies of magnetic materials [11] can determine the correct procedure to derive the dynamic susceptibility for many magnetic layered structures such as NiO and magnetic superlattices.

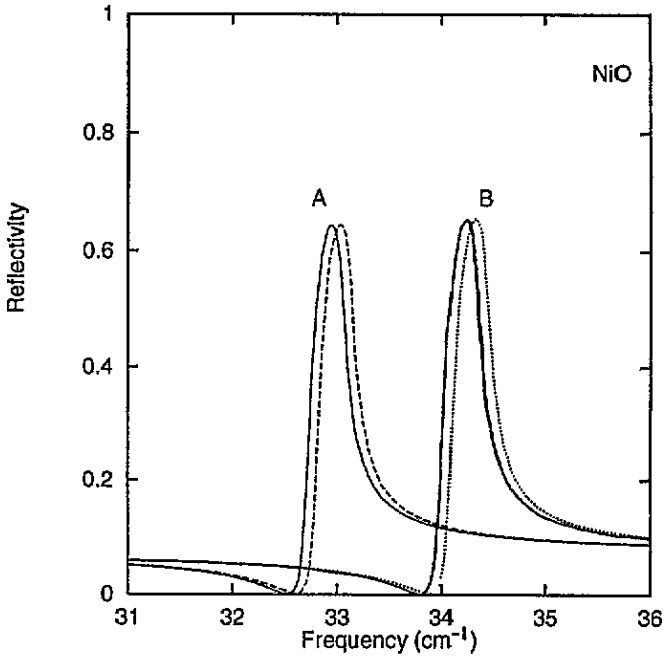

Figure 8. The computed oblique incidence (45°) reflectivity off NiO in p polarization, given by equation (30). We have made use of the magnetic permeability tensor derived in different procedures [1]: A, constant-h, or conventional analysis; B, h/b analysis. In both sets of curves, $H_0 = 2$ T (solid lines) and $H_0 = 5$ T (dashed/dotted lines); damping of 0.05 cm^{-1} is assumed.

For the sake of completeness we also show the s polarization 45° reflectivity off NiO in figure 9, where both methods lead to identical spectra. The reflectivity curve for $H_0 = 5$ T can be understood by reference to the corresponding scan line shown in figure 2. At the lowest frequency scan line falls in a continuum region and R is small. For $\omega \approx 5.5$ cm^{-1} the scan line leaves the continuum and enters a region where coupling to bulk modes cannot occur. Consequently R increases rapidly to $R \approx 1$. For $\omega \approx 12$ cm^{-1} the scan line enters the next bulk continuum region and R drops rapidly. In other words, the reflectivity has the classic *reststrahl* form as also seen in figure 8 for p polarization. The frequency scale is set by ω_+, equation (6), and therefore increases as H_0 increases. The frequency range is accessible, though with considerable difficulty, to far-infrared spectroscopy [19]. We believe that a series of measurements under various conditions (e.g. in a range of fields) on s polarization reflectivity would enable us to characterize the layered antiferromagnet NiO.

5. Conclusions

In this paper we have presented a full theoretical discussion of the surface polaritons, ATR and reflectivity spectra of layered antiferromagnets. Calculations are presented and illustrated numerically using the experimental magnetic parameters of NiO, which is an easy-plane antiferromagnet of the form shown in figure 1. The conventional calculation of μ for this material has recently been argued to be incorrect [1]. The alternative or h/b method [1] is consistent with the requirements of macroscopic electrodynamics. The two methods disagree only over the correct form of μ_{zz}. In this work we discuss how the difference in μ_{zz} for a

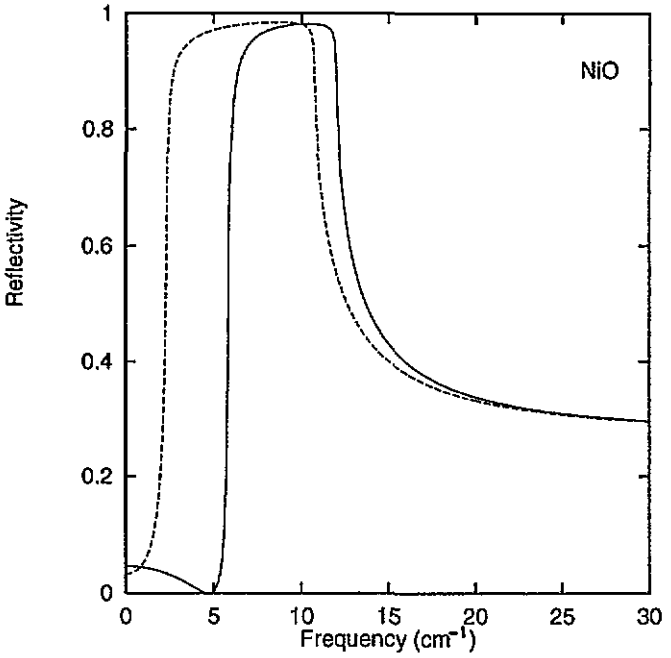

Figure 9. Calculated oblique incidence (45°) reflectivity off NiO in s polarization with $\Gamma = 0.05$ cm^{-1}, $H_0 = 2$ T (dashed lines) and $H_0 = 5$ T (solid lines).

layered antiferromagnet can be tested experimentally; we show calculated dispersion, ATR and oblique incidence reflectivity curves with particular reference to NiO.

The essential question may be phrased thus: given a crystal of NiO, say, is it possible to characterize the crystal, that is, determine the magnetic parameters, with s polarization measurements, then use the values of these parameters to discriminate between the alternative expressions for μ_{zz} by analysing measurements in p polarization? As seen from equations (2)–(5), the parameters are H_e, H_a, M_s and a damping constant Γ; the dielectric constant ε enters the expression for the reflectivity. In practice the angle of incidence ϕ in a reflectivity or ATR experiment is likely to be fixed for practical reasons but the external field H_0 does offer a degree of freedom. Computed s polarization *characterization* spectra are shown in figures 5, 6 and 9. These are drawn for $\Gamma = 0.05$ cm^{-1}, which is typical of a good crystal of FeF_2 [12, 13]. The frequencies for the particular case of NiO are at the low end of the range that is accessible to Fourier transform spectroscopy, but they are not impractical [19]. The computed p polarization spectra, figures 7 and 8, have features differing in position by about 1 cm^{-1} for the alternative forms of μ_{zz}. This is already clear from the polariton dispersion curves of figure 2. We believe that the s polarization spectra, figures 5, 6 and 9, contain sufficient sharp features to enable the five parameters H_e, H_a, M_s, Γ and ε to be determined with an accuracy for the frequencies $\omega_e = \gamma H_e$ etc considerably better than 1 cm^{-1}. This is certainly the case for FeF_2, where small variations in the parameters lead to significantly worse fits to data [12, 13]. The experimental resolution 0.02 cm^{-1} at best, is no restriction. In our view, therefore, the calculations in this paper show that the question of the correct form of μ can be resolved solely by measurement of far-infrared spectra. It is hoped that the experimental test of this basic question in magnetic spectroscopy will soon be forthcoming.

Acknowledgments

KA acknowledges financial support from Proyek PS2PT DEPDIKBUD (Bank Dunia XXI) Indonesia. We have benefited from helpful discussions with Bob Camley, Terry Parker and Stephen Smith.

References

[1] Stamps R L, Camley R E, Nörtemann F C and Tilley D R 1993 *Phys. Rev.* B **48** 15 470
[2] Cottam M G and Tilley D R 1989 *Introduction to Surface and Superlattice Excitations* (Cambridge: Cambridge University Press)
[3] Raj N and Tilley D R 1987 *Phys. Rev.* B **36** 7003
[4] Almeida N S and Mills D L 1988 *Phys. Rev.* B **38** 6698
[5] Kondoh H 1960 *J. Phys. Soc. Japan* **15** 1970
[6] Sievers A J and Tinkham M 1963 *Phys. Rev.* **129** 1566
[7] Morrish A H 1965 *The Physical Principles of Magnetism* (New York: Wiley)
[8] Hutchings M T and Samuelsen E J 1972 *Phys. Rev.* B **6** 3447
[9] Lockwood D J, Cottam M G and Baskey J H 1992 *J. Magn. Magn. Mater.* **104–107** 1053
[10] Grimsditch M, Sudha Kumar and Goldman R S 1994 *J. Magn. Magn. Mater.* **129** 327
[11] Dumelow T, Brown D E and Parker T J 1993 *18th Int. Conf. on Infrared and Millimeter Waves; Proc. SPIE* **2104** 633
[12] Brown D E, Dumelow T, Parker T J, Abraha K and Tilley D R 1994 *Phys. Rev.* B **49** 12 266
[13] Abraha K, Brown D E, Dumelow T, Parker T J and Tilley D R 1994 *Phys. Rev.* B **50** 6808
[14] Dumelow T, Parker T J, Smith S R P and Tilley D R 1993 *Surf. Sci. Rep.* **17** 151
[15] Almeida N S and Tilley D R 1990 *Solid State Commun.* **73** 23
[16] Camley R E 1987 *Surf. Sci. Rep.* **7** 103
[17] Hartstein A, Burstein E, Maradudin A A, Brewer R and Wallis R F 1973 *J. Phys. C: Solid State Phys.* **6** 1266
[18] Fonseca T L, Carrico A S and Almeida N S 1992 *Phys. Rev.* B **46** 11 626
[19] Parker T J private communication